Proceedings of the International Conference on Numerical Heat Transfer and Fluid Flow (NHTFF-2020)
NIT Warangal, India – Jan 17-19, 2020.

FERROMAGNETIC AND NON-MAGNETIC NANO-PARTICLES IN NANOFLUID FLOW FROM A STRETCHING CYLINDER WITH MAGNETIC INDUCTION: SPECTRAL RELAXATION SOLUTION

MD. Shamshuddin[1a], M. Ferdows[2b], Rezwan[2c] , O. Anwar Beg[3d], A. Kadir[3e]
[a]*Department of Mathematics, Vaagdevi College of Engineering, Warangal-506005, Telangana, India.*
[b,c] *Department of Applied Mathematics, University of Dhaka, Dhaka-1000, Dhaka, Bangladesh.*
[d,e] *Department of Mechanical/Aeronautical Engineering, University of Salford, Manchester-M54WT, UK.*

*Corresponding author Email: shammaths@gmail.com

Received: November 29, 2019 Accepted: December 6th 2019

Abstract

This paper studies the boundary layer flow and heat transfer in an incompressible viscous electrically conducting nanofluid containing ferroparticles or non-magnetic nanoparticles external to a stretching cylinder in the presence of magnetic induction. We consider water as a base fluid embedded with the two types of nanoparticles namely magnetic (Manganese Franklinite (Mn-$ZnFe_2O_4$), Ferric Oxide (Fe_3O_4)) and non-magnetic (Silicon Dioxide (SiO_2), Nimonic 80a). The governing non-linear partial differential equations and associated wall and free stream boundary conditions are reduced to a set of non-linear ordinary differential equations with appropriate boundary conditions using similarity transformation. The resulting equations are solved numerically using an efficient, stable, spectral relaxation method (SRM). The SRM code is validated with available solutions in the literature for limiting cases and excellent agreement is achieved. The emerging boundary value problem is shown to be controlled by various magnetic, geometrical and nanoscale parameters. The impact of these parameters on momentum and heat transfer characteristics are visualized graphically and tabulated with comprehensive discussion. The local skin friction and local Nusselt number are also presented graphically. The convergence rates achieved with standard SRM and SRM with SOR (successive over relaxation) are also studied and the latter is observed to achieve faster convergence. The SRM simulations show that with higher values of reciprocal of magnetic Prandtl number (stronger magnetic diffusion relative to viscous diffusion) the boundary layer flow is decelerated whereas the temperature is enhanced (thicker thermal boundary layer). Higher acceleration is attained with non-magnetic nanoparticles (SiO_2) whereas the best thermal enhancement is obtained with magnetic nanoparticles (Fe_3O_4). Substantial acceleration of the flow is also achieved with greater cylinder curvature parameter and enhanced magnetic induction and temperature elevation is also produced.

Keywords: *Electromagnetic induction; metallic nanoparticles; coating boundary layers; stretching cylinder; spectral relaxation method (SRM).*

1. Introduction

Boundary layer flow and heat transfer has numerous process engineering applications including coating dynamics, polymer sheet extrusion, near-wall flows in fuel cell synthesis and enrobing systems. Boundary-layer theory has the advantage that while it greatly simplifies the Navier-Stokes viscous flow equations, it retains physical accuracy. The boundary layer behaviour on moving surfaces (conveyor belts) was first explored by Sakiadis [1,2]. Crane [3] extended Sakiadis's work to examine the steady-state incompressible boundary layer flow from a stretching surface due to a moving stretching surface with a constant surface temperature in an ambient fluid. He also considered the case when the velocity varies linearly with the distance from a fixed point and derived a closed-form similarity solution. Many researchers subsequently modified the Crane-Sakiadis model to

consider other effects including wall suction/injection, heat flux, magnetic fields, exponential sheet stretching, porous media and radiative heat transfer. Representative works in this regard include Gupta and Gupta [4], Dutta et al. [5], Bég et al. [6] and Uddin et al. [7]. The above studies were confined to horizontal or vertical stretching surfaces and *neglected curvature*. Many engineering components are inherently curved and therefore require boundary layer coating models which incorporate curvature effects. For example, Schwarz and Wediner [8] have shown that surface curvature is equivalent to an applied time-independent overpressure distribution in liquid paint coating flows. Magyari et al. [9] emphasized the significant modifications in surface skin friction and heat transfer rates caused by curvature. The situation is further complicated when the cylinder surface is extending (or contracting), a process encountered in blow moulding, pipe fabrication etc. [10-13]. Wang [14] derived analytical solutions for steady Newtonian flow over a stretching cylinder using a similarity transformation. Ishak et al. [15] studied numerically the hydromagnetic convection flow from a stretching cylinder with the Keller box finite difference method and evaluated the effect of magnetic parameter, Prandtl number and Reynolds number on the velocity and temperature fields. Dispersing high thermal conductivity solid particles in conventional heat transfer fluids can significantly enhance the thermal conductivity of the resulting combined suspensions. "Nanofluids" therefore, as first proposed by Choi [16] at Argonne Energy Lab, USA, represent engineered colloids consists of nanoparticles dispersed in a base fluid. The nanoparticles used in synthesis of nanofluids are typically metallic (Al, Cu), metallic oxides (Al_2O_3, TiO_2), nitrides (AlN, SiN), carbides (SiC) or carbon nanotubes with diameters ranging between 10 and 100nm. Sandeep et al. [17] studied unsteady natural convective flow of Nimonic 80a (nickel chromium iron alloy)-Ethylene glycol nanofluid from an infinite vertical plate observing that with an alteration in nanoparticle shape the heat transfer rate is elevated. Pandey and Kumar [18] examined the boundary layer flow and heat transfer of Cu-water nanofluid flow from a stretching cylinder with slip. In recent years, magnetic and super magnetic nanofluids have emerged as a new sub- group of nanofluids which exhibits both magnetic and thermal enhancement property. This type of nanoparticle has extensive applications in biomedicine, thin film smart polymer coatings, magneto-nanofluid heat pipes and smart nuclear bio-inspired pumping systems. Many researchers have developed robust mathematical models of magnetic nanoparticle flows using rigorous experimental data as a foundation. Bég et al. [19] studied computationally the nonlinear, steady, forced convection, hydromagnetic flow of electro-conductive magnetic nano-polymer with magnetic induction effects for four different magnetic nanoparticles and three different base fluids. However, *to the authors' knowledge, the flow and heat transfer of ferro-nanofluid over a stretching cylinder with magnetic induction and different magnetic and non-magnetic nanoparticles, has thus far not been explored in the scientific literature*. This is the focus of the present study. The scenario considers a static magnetic field applied parallel to the stretching cylinder longitudinal axis i.e. the magnetic field is aligned with the cylinder. Via similarity scaling transformations, the nonlinear multi-physical boundary value problem is transformed from a system of partial differential equations to ordinary differential equations with appropriate wall and free stream conditions. The spectral relaxation method (SRM) is utilized to solve the ordinary differential boundary value problem with faster convergence rates. The simulations may find applications in coating of engineering components with magnetic nanomaterials.

2. Mathematical Model

We consider the axisymmetric, steady, two-dimensional laminar boundary layer incompressible

flow of a water-based (aqueous) nano-ferrofluid over a stretching cylinder. The x-axis is measured along the axis of the cylinder and *r*-axis is orientated in the radial direction. The effect of magnetic induction is taken into account since magnetic Reynolds number is adequately large and magnetic field is therefore distorted by the flow [20]. The magnetic field is aligned with the cylinder axis and comprises two mutually perpendicular components, $\bar{H}(H_1, H_2)$.The normal component of the induced

magnetic field, H_2 vanishes at the wall and the parallel component, H_1 approaches to the given value $H_e = xH_0$ at the edge of the boundary layer (free stream).The wall temperature is T_w and the free stream temperature is T_∞. The physical model is illustrated in **Figure 1.** The cylinder is electrically non-conducting and electrical field, polarization, viscous and Ohmic dissipation effects are negated. Further, it is assumed that cylinder is being stretched in the axial direction with linear velocity, $U_w = U_0(x/l)$ where U_0 is constant and l is the characteristic dimension (e.g. cylinder length). Under above assumptions, the governing continuity, magnetic induction, momentum and heat conservation equations for magnetohydrodynamic nano-ferrofluid boundary layer forced convection external to the cylinder, may be written, extending the models in [15, 21] as:

$$\frac{\partial(ru)}{\partial x} + \frac{\partial(rv)}{\partial r} = 0 \tag{1}$$

$$\frac{\partial(H_1 r)}{\partial x} + \frac{\partial(H_2 r)}{\partial r} = 0 \tag{2}$$

$$u\frac{\partial u}{\partial x} + v\frac{\partial u}{\partial r} - \frac{\mu_e}{4\pi\rho_f}\left(H_1\frac{\partial H_1}{\partial x} + H_2\frac{\partial H_2}{\partial r}\right) = \frac{\mu_{nf}}{\rho_{nf}}\left(\frac{\partial^2 u}{\partial r^2} + \frac{1}{r}\frac{\partial u}{\partial r}\right) \tag{3}$$

$$u\frac{\partial H_1}{\partial x} + v\frac{\partial H_1}{\partial r} - H_1\frac{\partial u}{\partial x} - H_2\frac{\partial u}{\partial x} = \eta_0\left(\frac{\partial^2 H_1}{\partial r^2} + \frac{1}{r}\frac{\partial H_1}{\partial r}\right) \tag{4}$$

$$u\frac{\partial T}{\partial x} + v\frac{\partial T}{\partial r} = \frac{k_{nf}}{(\rho c_p)_{nf}}\left(\frac{\partial^2 T}{\partial r^2} + \frac{1}{r}\frac{\partial T}{\partial r}\right) \tag{5}$$

The following velocity, magnetic induction and temperature boundary conditions are prescribed at the wall and in the free stream:

$$\left.\begin{array}{l} At\ \ r = a,\quad u = U_w,\ v = 0,\ \dfrac{\partial H_1}{\partial r} = H_2 = 0,\ T = T_w \\ As\ \ r \to \infty,\ u \to 0,\quad v = 0,\quad H_1 \to H_e,\ \ T \to T_\infty \end{array}\right\} \tag{6}$$

Here *u* and *v* are the velocity components along the *x* and *r* directions, Temperature is denoted by T, ρ_{nf} is the density of the nanofluid, μ_{nf} is the dynamic viscosity of the nanofluid and α_{nf} is the thermal diffusivity of the nanofluid. To simulate the modified properties of the nanofluid, we define the density of the nanofluid ρ_{nf}, the dynamic viscosity of the nanofluid μ_{nf}, the thermal diffusivity of the nanofluid α_{nf} respectively as [15] :

$$\left.\begin{array}{l} \mu_{nf} = \dfrac{\mu_{nf}}{(1-\phi)^{2.5}},\ \rho_{nf} = (1-\phi)\rho_f + \phi\rho,\ \upsilon_{nf} = \dfrac{\mu_{nf}}{\rho_{nf}},\ (\rho c_p)_{nf} = (1-\phi)(\rho c_p)_f + \phi(\rho c_p)_s,\ \dfrac{k_{nf}}{k_f} = \dfrac{(k_s + 2k_f) - 2\phi(k_f - k_s)}{(k_s + 2k_f) + \phi(k_f - k_s)} \end{array}\right\} \tag{7}$$

For simplicity, we introduce the following transformations in the non-dimensional equations (1)-(6):

$$\left.\begin{array}{l} \psi(x,r) = \left(\sqrt{\upsilon_f U_w x}\right) a\ f(\eta),\ \eta(x,r) = \dfrac{r^2 - a^2}{2a}\left(\sqrt{U_W/\nu_f x}\right), T_w = T_\infty + T_0(x/l), \theta(\eta) = (T - T_\infty)/(T_W - T_\infty) \end{array}\right\} \tag{8}$$

Here $\psi(x,r)$ is the stream function and $\eta(x,r)$ is the dimensionless similarity variable, f and g are dimensionless stream and magnetic stream functions respectively and θ is dimensionless temperature function. For the velocity field we define the dimensionless steam function, $\psi(x,r)$ as follows:

$$\left.\begin{array}{l} u = \dfrac{1}{r}\dfrac{\partial\psi}{\partial r},\ v = -\dfrac{1}{r}\dfrac{\partial\psi}{\partial x} \end{array}\right\} \tag{9}$$

After using the above similarity variables, the governing dimensionless boundary layer equations for momentum, magnetic induction and energy for the regime emerge as:

$$\left(1+2\gamma\eta\right)f'''+2\gamma f''+\left(1-\phi\right)^{2.5}\left\{\left(1-\phi\right)+\phi\frac{\rho_S}{\rho_f}\right\}\left[f f''-f'^2+\beta\left(g'^2-g g''\right)\right]=0 \tag{10}$$

$$\lambda\left(1+2\gamma\eta\right)g'''+2\gamma\lambda g''+\left[f g''-f'' g\right]=0 \tag{11}$$

$$\frac{k_{nf}}{k_f}\left[\left(1+2\gamma n\right)\theta''+2\gamma\theta'\right]+\Pr\left[\left(l-\phi\right)+\phi\frac{\left(\rho c_p\right)_s}{\left(\rho c_p\right)_f}\right]\left(f\theta'-f'\theta\right)=0 \tag{12}$$

Proceeding with the analysis we define:

$$\phi_1=\left(1-\phi\right)^{2.5}\left\{\left(1-\phi\right)+\phi\frac{\rho_s}{\rho_f}\right\},\qquad \phi_2=\left[\left(l-\phi\right)+\phi\frac{\left(\rho c_p\right)_s}{\left(\rho c_p\right)_f}\right] \tag{13}$$

Eqns. (10)-(12) thereby assume the final form:

$$\left(1+2\gamma\eta\right)f'''+2\gamma f''+\phi_1\left[\left(f f''-f'^2\right)+\beta\left(g'^2-g g''\right)\right]=0 \tag{14}$$

$$\lambda\left(1+2\gamma\eta\right)g'''+2\gamma\lambda g''+\left[f g''-f'' g\right]=0 \tag{15}$$

$$\frac{k_{nf}}{k_f}\left[\left(1+2\gamma n\right)\theta''+2\gamma\theta'\right]+\Pr\ \phi_2\left(f\theta'-f'\theta\right)=0 \tag{16}$$

Where primes denote the differentiation with respect to η. Now the transformed boundary conditions assume the form:

$$\begin{aligned}&\eta=0,\qquad f(0)=0,\ f'(0)=1,\ \theta(0)=1,\ \ g(0)=0,\ g''(0)=0,\\&\eta\to\infty,\qquad f'(\infty)\to 0,\qquad \theta(\infty)\to 0,\qquad g'(\infty)\to 1\end{aligned} \tag{17}$$

In Eqns. (14)-(17), γ is the curvature parameter, *Pr* is the Prandtl number, β is the magnetic (body force) parameter and λ is the reciprocal of the Prandtl number, which are respectively defined as:

$$\gamma=\left(\sqrt{\frac{l\upsilon_f}{U_0a^2}}\right),\beta=\frac{\mu_e}{4\pi\rho_f}\left(\frac{H_o l}{U_o}\right)^2,\lambda=\frac{\eta_0}{\upsilon_f},\Pr=\frac{\mu_f}{\rho_f}\frac{\left(\rho c_p\right)}{k_f} \tag{18}$$

In view of the velocity field the local skin friction coefficient and the local Nusselt number in dimensionless form are given by:

$$\mathrm{Re}_x^{1/2}C_f=\frac{1}{(1-\phi)^{2.5}}f''(0),\mathrm{Re}_x^{-1/2}Nu_x=-\theta'(0) \tag{19}$$

3. Numerical Solution with SRM

The spectral relaxation method is a numerical technique based on simple iteration scheme formed by reducing large systems of nonlinear equations into smaller systems of linear equations, using spectral collocation. Motsa [22] has described this method in detail. SRM is equally adept at accommodating coupled nonlinear systems of ordinary or partial differential equations. Using the SRM technique we discretize the transformed Eqns. (14) to Eq. (17). This process involves 3 stages:

1. Reduction of the order of the momentum equation for $f(\eta)$ by introducing the transformation $f'(\eta)=F(\eta)$ and expression of the original equation in terms of $F(\eta)$
2. Assuming that $f(\eta)$ is known from the previous iteration (denoted by $f_r(\eta)$), an iteration scheme is constructed for $F(\eta)$ by assuming that only *linear* terms in $F(\eta)$ are to be evaluated at the current iteration level (denoted by $F_{r+1}(\eta)$) and all other terms (linear and nonlinear) are assumed to be known from the previous iteration. In addition, nonlinear terms in $F(\eta)$ are evaluated at the previous iteration.

3. The iteration schemes for the other governing dependent variables are developed in a similar manner, however using the updated solutions of the variables determined in the previous equation.

The strategy described above is analogous to the Gauss-Seidel technique for decoupling linear algebraic systems of equations. Using this algorithm leads to a sequence of linear differential equations with variable coefficients which can be easily be solved using standard numerical techniques for linear differential equations e.g. Chebyshev spectral collocation methods ([23], [24]).Spectral methods are preferred here owing to their remarkably high accuracy and ease of implementation in discretization and the subsequent solution of variable coefficient linear differential equations with smooth solutions over simple domains.

A comparison table between the basic SRM and the SRM with SOR is given in **Table 1** for Nusselt number (for the 4 different nanoparticles studied). It is clear that SRM with SOR accelerates the convergence.

Table 1: Comparison of Nusselt number convergence between SRM and SRM with SOR.

Parameters	**Nano Particles**	**Nusselt number**	**Iterations**	
			SRM	**SRM with SOR**
$\gamma = 0.5, \beta = 0.14, \lambda = 0.5, \phi = 0.1, 0.15, \Pr = 0.72$	Mn-$ZnFe_2O_4$	0.14	37	19
$\gamma = 0.5, \beta = 0.1, \lambda = 0.5, \phi = 0.1, 0.15, \Pr = 0.72$	SiO_2	1.2356	38	21
$\gamma = 1.1, \beta = 0.1, \lambda = 0.5, \phi = 0.1, 0.15, \Pr = 0.72$	Nimonic 80a	1.1249	33	15
$\gamma = 0.5, \beta = 0.1, \lambda = 0.5, \phi = 0.1, 0.15, \Pr = 0.72$	Fe_3O_4	1.2233	35	20

4. SRM Results, Validation and Discussion

An extensive number of SRM computations have been presented in **Figs. 2-11**. The thermophysical properties of base fluid (water) and 4 different nanoparticles (two magnetic (Fe_3O_4, Mn-$ZnFe_2O_4$) and two non-magnetic (Nimonic 80a, SiO_2)) are taken from ([21, 25]). The accuracy of spectral relaxation method (SRM) code (which is executed in Matlab symbolic software) is verified by benchmarking with simpler models from published works in the literature. Taking $\phi_1 = \phi_2 = 1 = k_{nf}/k_f$, $\phi = \gamma = \lambda = \beta = 0$ and varying the value of $\Pr$, the SRM solutions are compared for Nusselt number with Keller-box finite difference solutions of Khan and Pop [26] and asymptotic solutions of Wang [27]. The results are found to be an excellent agreement as shown in the **Table 2.** Confidence in the SRM code is therefore justifiably high. $\Pr < 1$ corresponds to low thermal conductivity fluids, $\Pr = 7$ to water and $\Pr > 20$ to polymers.

Table 2: Comparison of present results with published for different values of $\Pr$

Pr	Present Study	Wang [27]	Khan and Pop [26]
0.2	0.16911012	0.1697	0.1691
0.7	0.45391616	0.4539	0.4539
2	0.91135768	0.9114	0.9114
7	1.89540305	1.8954	1.8954
20	3.35390414	3.3539	3.3539
70	6.46218077	6.4622	6.4622

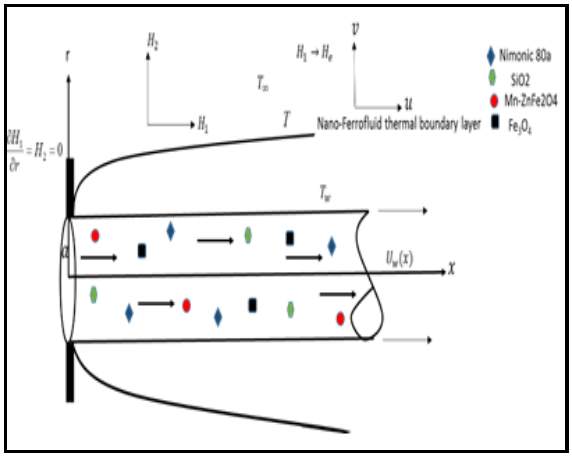

Fig. 1. Physical model and Coordinate system

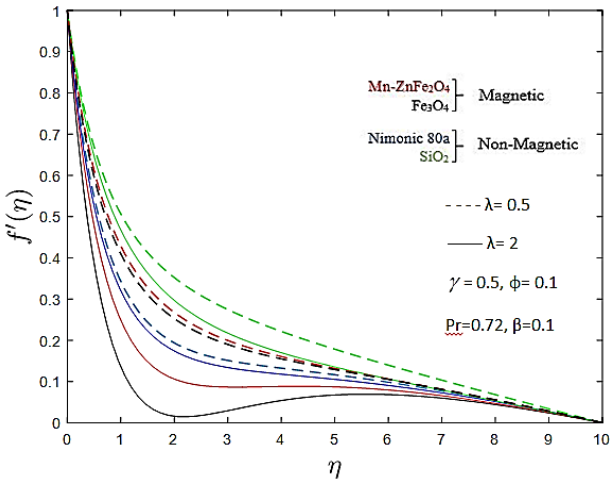

Fig. 2. Velocity profiles, $f'(\eta)$ for various reciprocal of magnetic Prandtl number (λ)

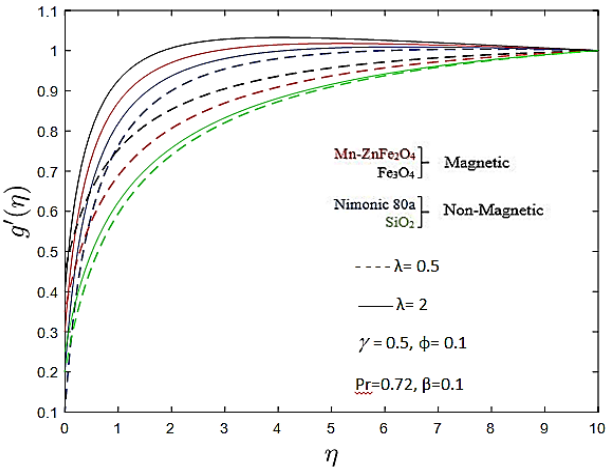

Fig. 3. Magnetic stream function gradient, $g'(\eta)$ for various reciprocal of magnetic Prandtl number (λ)

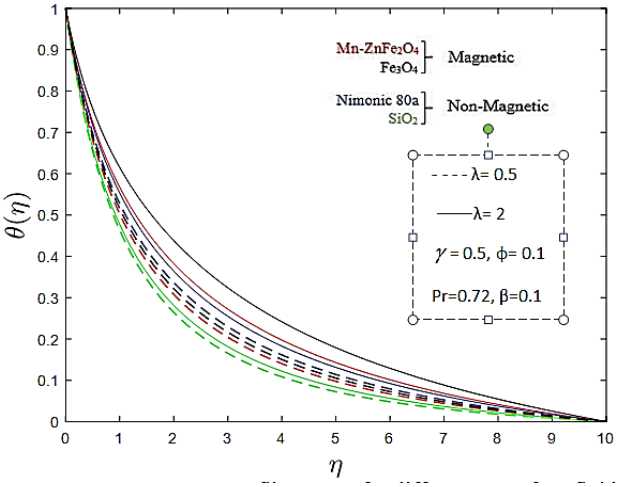

Fig. 4. Temperature profiles, $\theta(\eta)$ for various reciprocal of magnetic Prandtl number (λ)

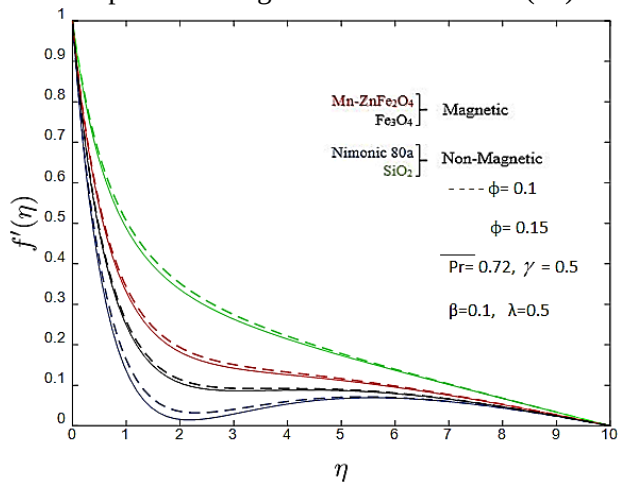

Fig. 5. Velocity profiles, $f'(\eta)$ for various nanoparticle solid volume fractions (ϕ)

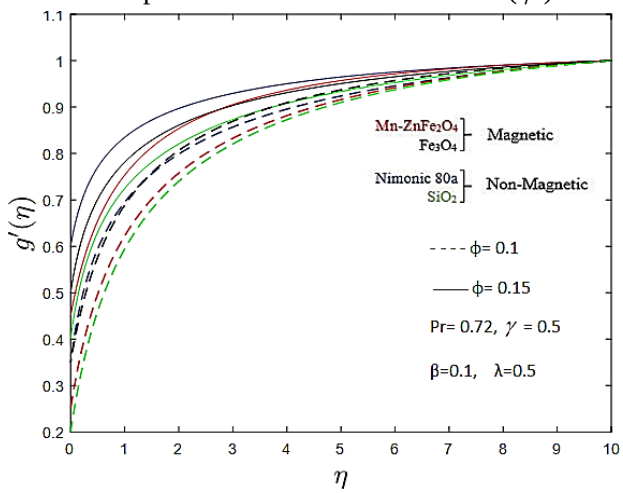

Fig. 6. Magnetic stream function gradient, $g'(\eta)$ for various nanoparticle solid volume fractions (ϕ)

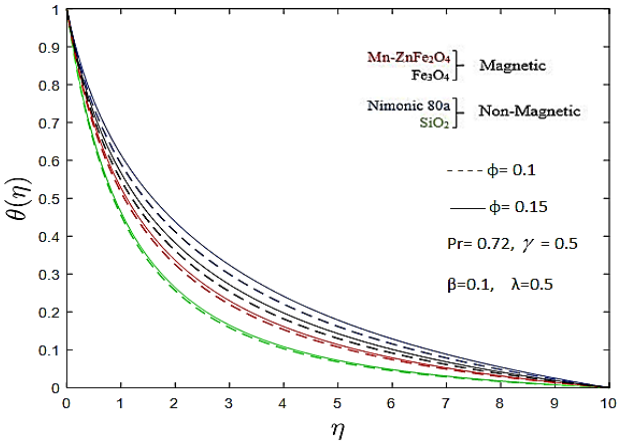

Fig. 7. Temperature profiles, $\theta(\eta)$ for various nanoparticle solid volume fractions (ϕ)

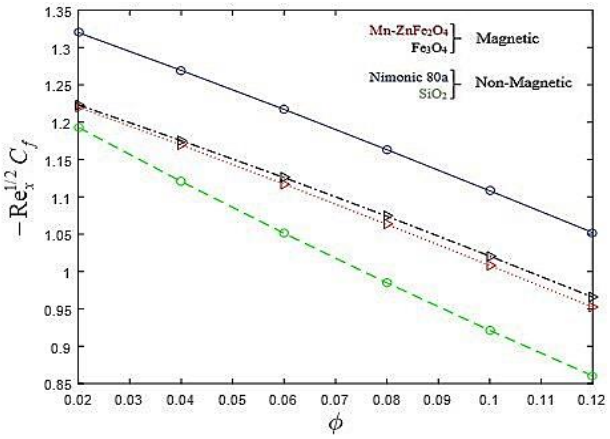

Fig. 8. Surface shear stress distribution, $f''(0)$ versus nanoparticle solid volume fraction (ϕ)

Fig. 2 shows that velocity $f'(\eta)$ in the boundary layer is strongly decreased with higher values of λ increases. Non-magnetic nanoparticle SiO_2 achieve the highest velocity whereas magnetic nanoparticle Fe_3O_4 achieve the lowest velocity. The other two nanoparticles produce velocities between these two extremes and Nimonic 80a is higher than Mn-$ZnFe_2O_4$ for large values of λ. **Fig. 3** displays the influence of λ on induced magnetic field distributions, $g'(\eta)$. As the values of λ increases there is a boost in magnetic stream function gradient. In all cases the profiles tend asymptotically to unity in the free stream. The parameter λ is the reciprocal of this ratio i.e. magnetic diffusion rate divided by viscous diffusion rate. When magnetic diffusion dominates this exacerbates the magnetic induction effect and explains the higher magnitudes of $g'(\eta)$ achieved for $\lambda = 2$ (thicker magnetic boundary layer) and the suppressed magnitudes corresponding to $\lambda = 0.5$ (thinner magnetic boundary layer) in fig. 3. Maximum $g'(\eta)$ values are attained for Fe_3O_4 nanoparticles followed by Mn-$ZnFe_2O_4$, then Nimonic 80a and finally SiO_2. Clearly ferromagnetic characteristics are beneficial to magnetic induction. **Fig. 4** shows that for large value of λ there is a distinct elevation in temperature. Stronger magnetic diffusion relative to viscous (momentum) diffusion is therefore assistive to the thermal diffusion process also. Magnetic nanoparticles achieve significantly greater heat transfer enhancement compared with non-magnetic nanoparticles i.e. maximum temperatures are produced with Fe_3O_4 followed by Mn-$ZnFe_2O_4$, then Nimonic 80a and finally non-metallic SiO_2.

Figs. 5-7 present the velocity, magnetic stream function gradient and temperature profiles with transverse coordinate for a change in solid volume fraction parameter, ϕ, and different nanofluid suspensions. 10% and 15% doping concentrations are studied ($\phi = 0.1, 0.15$). From Fig. 5 it is evident that there is a slight deceleration in flow with greater volume fraction i.e. momentum boundary layer thickness is decreased. The non-magnetic nanomaterial SiO_2 achieves the highest velocity, followed by Mn-$ZnFe_2O_4$, Fe_3O_4 and Nimonic 80a respectively. The magnetic stream function gradient (fig. 6) however is significantly enhanced with an increase in solid volume fraction parameter and the effect is most prominent near the cylinder surface, progressively diminishing into the free stream. From Fig. 6 it is apparent that maximum magnetic stream function gradient is achieved by SiO_2 followed by Mn-$ZnFe_2O_4$, Fe_3O_4 and Nimonic 80a respectively. Fig. 7 shows that there is a relatively weak increase in nanofluid temperatures; the best thermal enhancement is attained by Nimonic 80a followed respectively by Fe_3O_4, Mn-$ZnFe_2O_4$ and SiO_2. Similar observations on temperature response have been reported by Noghrehabadi *et al.* [25] although in the absence of magnetic induction.

Fig. 8 illustrates the impact of solid volume fraction parameter ϕ on skin friction for all 4 nanoparticles investigated. The value of ϕ is chosen in the range 0.02 to 0.1 [21] and corresponds to 2% to 10% nanoparticle doping. As the value ϕ increases the shear stress coefficient decreases i.e.

strong flow deceleration is induced. Non-magnetic nanoparticle Nimonic 80a achieves the highest shear stress and the non-magnetic nanoparticle SiO_2 produces the lowest shear stress.

5. Conclusions

The present SRM numerical simulations have shown that:

- With greater reciprocal of magnetic Prandtl number the boundary layer flow is decelerated whereas the temperature magnitudes are enhanced. Maximum flow acceleration is achieved with non-magnetic nanoparticle SiO_2 and the best thermal enhancement is obtained with magnetic nanoparticle Fe_3O_4.
- Increasing nanoparticle solid volume fraction decelerates the flow both for magnetic and non-magnetic nanoparticles.
- Skin friction coefficient decreases with an increase in nanoparticle solid volume fraction parameter and reciprocal of magnetic Prandtl number.
- Nusselt number decreases with an increase in Prandtl number.

References

[1] B.C. Sakiadis, AIChE J. 7(1), 26-28 (1961).
[2] B.C. Sakiadis, AIChE J. 7(2), 221-225 (1961).
[3] L.J. Crane, ZAMP. 21(4), 645-647 (1970).
[4] P.S. Gupta, A.S. Gupta, Cana. J. Chem. Eng. 55(6), 744-746 (1977).
[5] B.K. Dutta, P. Roy, A.S. Gupta, Int. Commun. Heat Mass Transf. 12(1), 89-94 (1985).
[6] O. Anwar Bég et al., Appl. Nanosci. 4(8), 943-957 (2014).
[7] M.J. Uddin, O. Anwar Bég, M.N. Uddin, Energy. 115, 1119-1129 (2016).
[8] L.W. Schwartz, D.E. Weidner, J. Eng. Math. 29(1), 91-103 (1995).
[9] E. Magyari, B. Keller, I. Pop, ZAMM, 82(2), 142-144 (2002).
[10] R.E. Khyat, A. Derdouri, Int. J. Numer. Meth. Eng. 37(22), 3773-3791 (1994).
[11] Y.M. Luo, L. Chevalier, F. Utheza, ASME 2012 11th Biennial Conference on Engineering System Design and Analysis, (2012), July, Nantes, France.
[12] V.R. Prasad et al., AIAA J. Thermophys. Heat Transf. 28, 764-770 (2014).
[13] M. Faisal et al., AIP Adv. 6, 055316-1-055316-15 (2016).
[14] C.Y. Wang, Phys. Fluids. 31(3), 466-468 (1988).
[15] A. Ishak, R. Nazar, I. Pop, Ener. Conv. Mang. 49(11), 3265-3269 (2008).
[16] S.U.S. Choi *et al.*, Appl. Phys. Let. 79(14), 222-2254 (2001).
[17] N. Sandeep, V. Sugunamma, P. Mohankrishna, Adv. Phys. Theor. Applic. 23, 36-43 (2013).
[18] A.K. Pandey, M. Kumari, Alex. Eng. J. 56(4), 671-677 (2017).
[19] O. Anwar Bég et al. J. Nanoeng., Nanomat. Nanosyst. 233(1), 27-45 (2019).
[20] K.C. Cramer, S.I. Pai, Applied Magnetofluid Dynamics, MacGraw-Hill, USA (1973).
[21] M. Qasim, Z.H. Khan, W.A. Khan, I.A. Shah, PloS one, 9(1), e83930. doi.org/10.1371/journal.pone.0083930
[22] S.S. Motsa, Chem. Eng. Commun. 201(2), 241-256 (2014).
[23] N.A. Haroun, P. Sibanda, S. Mondal, S.S. Motsa, Boundary Value Probs. 2015 (1), 24. https://doi.org/10.1186/s13661-015-0289-5.
[24] C. Canuto, M.Y. Hussaini, A. Quarteroni, T.A. Zhang, Spectral Methods in Fluid Dynamics, Springer-Verlag, Berlin (1988).
[25] A. Noghrehabadi *et al.*, Int. J. Multidisc. Sci. Eng. 2(9), 18-21 (2011).
[26] W.A. Khan, I. Pop, Int. J. Heat Mass Transf. 53(11), 2477-2483, (2010).
[27] C.Y. Wang, ZAMM, 69(11), 418-420 (1989).